water

MDPI

Article

Analysis of Flow Loss Characteristics of a Multistage Pump Based on Entropy Production

Qi Meng [1], Guidong Li [1,2,*], Jieyun Mao [1,2,*], Danhua Zhao [3], Yutong Luo [1] and Tengfei Hou [1]

[1] Research Center of Fluid Machinery Engineering and Technology, Jiangsu University, 301 Xuefu Road, Zhenjiang 212013, China; mengqi0710@126.com (Q.M.); 17851559059@163.com (Y.L.); htf9227@163.com (T.H.)
[2] Wenling Fluid Machinery Technology Institute of Jiangsu University, Wenling 317525, China
[3] Taizhou Special Equipment Inspection and Testing Research Institute, Taizhou 318000, China; auto8787@163.com
* Correspondence: gdli@ujs.edu.cn (G.L.); mjygijon@163.com (J.M.); Tel.: +86-15061499603 (G.L.)

Abstract: To reveal the internal flow loss characteristics of a multi-stage pump, the unsteady calculation of the internal flow field of a seven-stage centrifugal pump was carried out, and the entropy production theory and Q criterion were utilized to analyze the unsteady flow characteristics of each flow component under different flow rates. The research results show that as the flow rate increases, the entropy production value and the energy loss inside the flow components also increase accordingly. The viscous dissipation entropy production caused by fluid viscosity is very small, and the turbulent dissipation entropy production caused by turbulent fluctuations and wall dissipation entropy production are the main sources of energy loss. The impellers, diffusers, and outlet chamber are the main regions of energy loss in the multistage pump. The entropy production value of the first-stage impeller is significantly higher than that of other impellers, while the entropy production value of the first-stage diffuser is significantly lower than that of other diffusers. Through vortex structure analysis, it is found that the high entropy production regions in the impeller are concentrated in the impeller inlet area, the blade suction surface, and the impeller outlet area.

Keywords: multistage pump; entropy production; Q criterion; energy dissipation; entropy production rate

check for updates

Citation: Meng, Q.; Li, G.; Mao, J.; Zhao, D.; Luo, Y.; Hou, T. Analysis of Flow Loss Characteristics of a Multistage Pump Based on Entropy Production. *Water* **2024**, *16*, 2974. https://doi.org/10.3390/w16202974

Academic Editor: Giuseppe Pezzinga

Received: 10 September 2024
Revised: 12 October 2024
Accepted: 16 October 2024
Published: 18 October 2024

Copyright: © 2024 by the authors. Licensee MDPI, Basel, Switzerland. This article is an open access article distributed under the terms and conditions of the Creative Commons Attribution (CC BY) license (https://creativecommons.org/licenses/by/4.0/).

1. Introduction

Multistage pumps are among the indispensable key equipment in fluid transportation systems, with their main function being to provide continuous and stable fluids and pressure to meet various industrial and civil demands. Multistage pumps achieve efficient fluid transportation through the series operation of multiple impellers and are widely used in water supply systems, petrochemical industry, mining, high-rise buildings, offshore platforms, etc. Multistage pumps provide sufficient head for the fluid by stepping up the pressure to adapt to different transportation heights and distances.

The structural design of multistage pumps is usually compact and small in size, which can achieve efficient fluid transportation in a limited space while maintaining low energy consumption and maintenance costs. Quantitative analysis of the energy loss and its distribution in various regions inside a multistage pump can more effectively optimize the geometric parameters of the multistage pump, thereby improving the performance and efficiency of the pump. Therefore, in-depth research on the energy loss characteristics of a multistage pump has important scientific value.

With the continuous advancement of Computational Fluid Dynamics (CFD) technology, the combination of numerical simulations and experiments has become the mainstream method for studying the internal flow characteristics of centrifugal pumps. Jafarzadeh et al. [1] conducted a three-dimensional flow simulation of a low-specific-speed centrifugal pump with different numbers of blades based on various turbulence models to

determine their effectiveness in flow rate prediction. The results indicated that, across all ranges, the seven-blade centrifugal pump exhibited the highest head coefficient compared to the five-blade and six-blade centrifugal pumps. The position of the blades relative to the volute tongue significantly affected the flow characteristics. Ji et al. [2] numerically simulated a single-blade centrifugal pump based on a new flow instability analysis method and defined the unsteady intensity and turbulence intensity in the rotor and volute domains to quantitatively study the instability of periodic flow. The results showed that the location and intensity of flow instability and turbulence in the rotor and stator domains can be directly displayed by averaging the results over the entire impeller rotation period. Shi et al. [3] studied the impact of different impeller outlet widths on the performance of multistage centrifugal pumps through numerical simulation, theoretical analysis, and experimental methods. The results showed that the numerical results were consistent with the trend of the experimental results, indicating that changing the impeller outlet width was a practical and convenient method to adjust the performance of multistage centrifugal pumps. Tan et al. [4] used CFD technology to conduct full-field steady multi-phase and unsteady transient numerical simulations of the internal flow of a centrifugal pump under multiple low-flow conditions. The study focused on analyzing the impact of phase angles in steady multi-phase calculations and time steps in unsteady calculations on head prediction results and compared the advantages and disadvantages of steady multi-phase and unsteady calculations for head prediction, as well as their causes. The results showed that the phase angle has little effect on the head prediction results of steady multi-phase numerical calculations, while the time step has a significant impact on the head prediction results based on unsteady numerical calculations. Sung et al. [5] analyzed the performance changes of a double-suction centrifugal pump based on numerical calculations and studied the effect of the surface roughness of pump components on pump performance. The results showed that the overall efficiency of the pump decreased by approximately 3.0% when the surface roughness was taken into account. Zheng et al. [6] conducted numerical simulations on centrifugal pumps with clearance flow and without clearance flow. The results showed that clearance flow caused the performance of the centrifugal pump to deteriorate, especially in terms of pressure fluctuation. Cui et al. [7] analyzed the unsteady flow inside a multistage centrifugal pump and the forces acting on the rotor components based on large eddy simulation (LES). The results showed that the different inlet velocity distributions were an important reason for the different head characteristics of each stage. The back-to-back impeller arrangement can effectively reduce axial force, and symmetrically distributed double tongues can reduce radial force and pump vibration. Researchers including Wu have introduced a multi-objective optimization approach that integrates experimental design, surrogate modeling, and optimization algorithms to enhance the performance of pumps by redesigning impellers and guide vanes [8]. Their findings indicated that at the design flow point, there was an increase of 8.8% in head and 2.8% in efficiency, along with a 1.34% reduction in CMEI, which is an auxiliary measure of the Minimum Efficiency Index. In another study, Zhang and colleagues conducted an intelligent optimization of a multi-stage pump's impeller outlet width, blade wrap angle, blade outlet angle, and guide vane inlet width using a Radial Basis Function (RBF) neural network [9]. The outcomes demonstrated a 4.35% increase in efficiency at the design condition, with a significant enhancement in the internal flow match between the optimized impeller and guide vane post-optimization. Zhang et al. [10] conducted simulations and analyses of the internal flow within a centrifugal pump to study the effects of different inlet pipes on the internal flow. The results indicated that different inlet flow angles significantly impact the internal flow of the centrifugal pump, leading to changes in the magnitude and direction of the radial force experienced by the pump impeller. Chen et al. [11] numerically analyzed the transient flow characteristics of a multistage centrifugal pump during the start-up process before system operation. The conclusion showed that the shorter start-up time intensifies the transient effect, the vortex structure shows periodic development and dissipation, and the

entropy production increases with the increase of impeller speed, reaching higher values in a shorter start-up time.

The production of entropy signifies the degree of irreversibility within a system and the extent of energy loss occurring in the flow dynamics. In recent years, this theory has seen certain developments in the assessment of energy loss in centrifugal pumps [12]. A large number of studies have shown that the entropy production theory can intuitively reflect the location of irreversible losses within the fluid and the spatial distribution of energy consumption, offering more advantages than traditional hydraulic loss assessments. It provides accurate and intuitive reference information for the subsequent improvement and optimization of hydraulic models [13–21]. Zhang et al. [22] used the local entropy production analysis method to evaluate the energy consumption loss during the operation of a centrifugal pump. Compared with the results calculated by the pressure drop method, the results of this method showed a certain deviation but were basically consistent in the entropy production of energy consumption in the impeller and volute domains of the centrifugal pump, indicating that the local entropy production method can be applied to the energy consumption evaluation of centrifugal pumps. Zhang et al. [23] used the second law of thermodynamics to propose a flow loss analysis method of the side channel pump based on entropy production and qualitatively analyzed the characteristics of the flow loss in a side channel pump. Jia et al. [24] employed the entropy production rate technique to forecast the dimensions and position of internal flow losses within a centrifugal pump, and they determined the vibrational energy distribution across various operating conditions using data from vibration tests. Cao et al. [25] demonstrated that entropy generation in rotating machinery is driven by factors such as fluid viscosity, turbulence fluctuations, and wall friction, with turbulence fluctuations and wall friction being the primary sources of energy dissipation. Lv et al. [26] used the entropy production theory and Q criterion method to study the installation angle of the volute tongue at different angles. The results showed that a reasonable increase in the installation angle of the volute tongue can reduce the backflow and the pressure pulsation at the volute tongue region, thereby reducing the energy loss and improving the energy utilization rate of the centrifugal pump. Qi et al. [27] applied the entropy production theory to analyze the performance and energy loss in a turbine, identifying flow separation and impingement due to the misalignment between the relative flow angle and the blade pitch angle as the predominant factors contributing to energy loss within the impeller. Zhang et al. [28] and his team used numerical simulation combined with entropy production theory to study the energy characteristics and flow features of an electrical submersible pump under different flow conditions. The results showed that the entropy production in the impellers and guide vanes of the electrical submersible pump first decreases and then increases as the flow rate increases, with the highest entropy production occurring in the guide vane part. In addition, the entropy production caused by velocity pulsation is the main factor causing energy loss.

Based on the entropy production theory and Q criterion, this paper numerically simulates and analyzes the distribution of the energy loss of each flow component of a multistage pump under different flow rates.

2. Numerical Simulation and Experimental Validation

2.1. Physical Model

In this study, a multistage centrifugal pump with six diffusers and seven impellers of eight 3D backward swept blades was chosen for the experiment. It is a multistage centrifugal pump of model PV 12X7-4, which is produced by Purity Pump Co., Ltd. (Taizhou, China). The entire flow domains were modeled in 3D using Pro/E. The main components of the model include the impellers, diffusers, front and rear pump chambers, inlet chamber, and outlet chamber. The primary design parameters of the model pump are listed in Table 1, and the 3D hydraulic model is shown in Figure 1.

Table 1. The main parameters of the model pump.

Design Parameter	Symbol	Value
Design flow rate	Q_d	12 m^3/h
Design head	H_d	70 m
Rotational speed	n	3500 r/min
Rated power	P	4 kW
Specific speed	n_s	131
Impeller inlet diameter	D_1	48.4 mm
Impeller outlet diameter	D_2	89 mm
Blade outlet width	b_2	6 mm
Impeller blade number	Z_i	8
Diffuser outlet diameter	D_0	117 mm
Diffuser blade number	Z_g	6
Inlet diameter of inlet chamber	D_{in}	51.4 mm
Outlet diameter of outlet chamber	D_{out}	50 mm

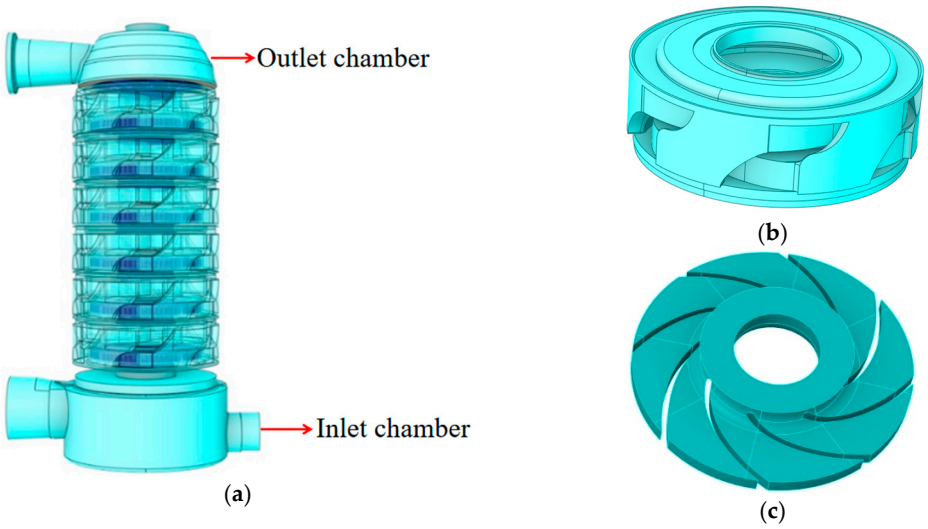
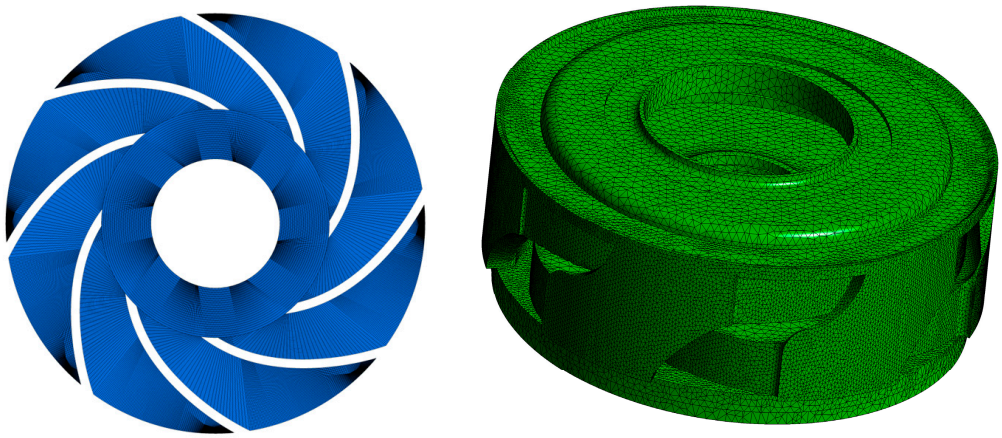


Figure 1. Three-dimensional diagram of the hydraulic model. (**a**) Multistage pump model; (**b**) Diffuser; (**c**) Impeller.

2.2. Numerical Calculation Method

Mesh generation is a critical step in finite element analysis, as it determines the convergence accuracy and speed of the simulation. In this study, ANSYS ICEM was used for meshing the flow components. The impeller domain was meshed with structured hexahedral elements, while the other computational domains, due to their complex structures, were meshed with unstructured tetrahedral elements that offer better applicability. Some mesh details are shown in Figure 2.

To ensure simulation accuracy and improve computational efficiency, mesh independence verification was conducted on a single-stage pump. The experimental head at the design point of the single-stage pump was 10 m. When the mesh number reached approximately 4.8 million elements, the head variation was very small and met the grid independence requirements in numerical simulation. Ultimately, the total mesh number for the multistage pump was set at approximately 22.2 million elements as the final computational mesh.



(**a**) (**b**)

Figure 2. Computational meshes of the impeller and diffuser. (**a**) Impeller domain mesh; (**b**) Diffuser domain mesh.

Considering the intricate structure of the multi-stage centrifugal pump, the three-dimensional transient incompressible Reynolds-averaged Navier-Stokes equations were coupled with the RNG *k*-*ε* turbulence model and can effectively simulate the internal flow of multistage centrifugal pumps [29–31]. Numerical simulations were performed using software ANSYS CFX 2022. Boundary conditions were configured with a mass flow inlet and a pressure outlet. The simulation utilized an MRF approach, treating the seven-stage impellers as the rotating region and the rest of the computational areas as stationary. Data transfer between the rotating and stationary domains was facilitated through interface surfaces. The convergence criterion was set to 10^{-5}. The ANSYS model settings are shown in Table 2.

Table 2. ANSYS model settings.

Setting	Type
Inlet boundary condition	Mass flow rate
Outlet boundary condition	Static pressure, 1 standard atmosphere
Solid wall surfaces	No-slip wall
Interface on both sides of impeller	Stage
Static and static interface	None
Convergence criterion	10^{-5}
Turbulence numerics	High resolution
Turbulence model	RNG *k*-*ε*

2.3. Experimental Validation

Experimental validation is one of the key methods to verify the reliability of numerical simulation results. The external characteristic test of the multistage pump in this study was conducted on a high-precision hydraulic machinery multifunctional test bench at the National Center for Quality Supervision and Inspection of Pump Product (Zhejiang). During the external characteristic test, the flow rates were measured at 13 operating points, with sufficient stabilization time between each point. Once the test data stabilized, measurements of the flow rate, head, rotational speed, and shaft power were recorded.

A schematic diagram of the test bench is shown in Figure 3. The system mainly consists of a multistage pump, a pipeline system, an electromagnetic flow meter, pressure sensors, and a data acquisition system. The key parameters of the main testing equipment are listed in Table 3. To minimize randomness and errors during the test, repeated tests of the flow rate–head data were conducted multiple times, as shown in Figure 4. The external

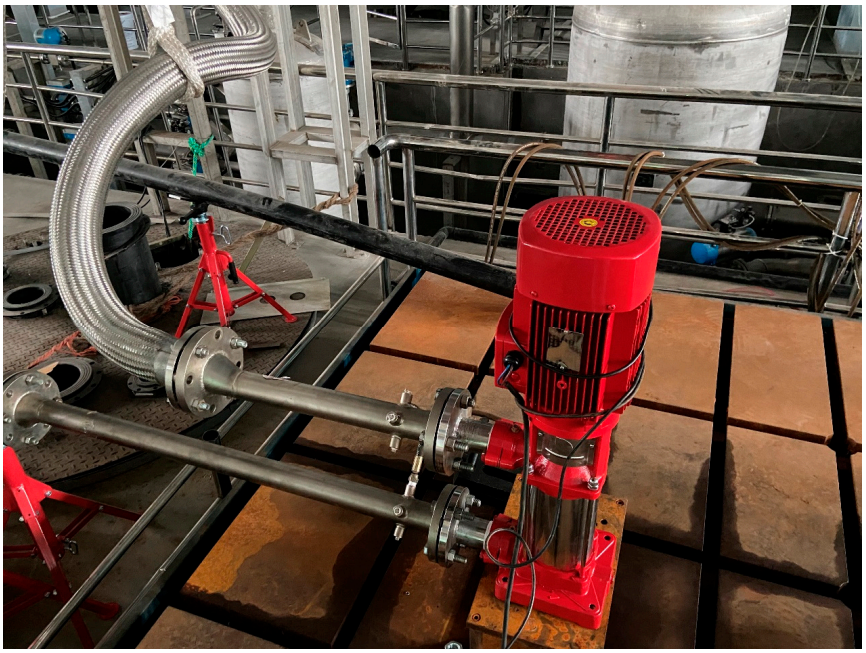
characteristics of the multistage pump were described using dimensionless flow rate ϕ and dimensionless head Ψ. The definitions are as follows:

$$\phi = Q/\pi D_2 b_2 u_2 \tag{1}$$

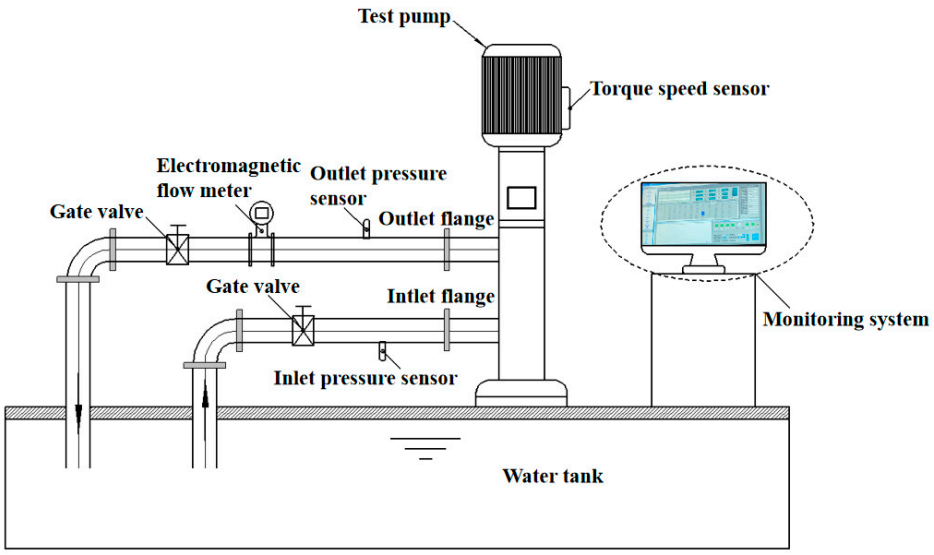
$$\Psi = 2gH/u_2^2 \tag{2}$$

$$u_2 = D_2 \pi n/60 \tag{3}$$

where u_2 is the impeller outlet circumference speed, ϕ is dimensionless flow coefficient, and Ψ is dimensionless head coefficient.



(**a**)



(**b**)

Figure 3. External characteristic testing device. (**a**) Multistage pump test bench; (**b**) Test bench schematic diagram.

Table 3. Main equipment parameters.

Test Equipment	Product Figure	Parameter
Electromagnetic Flow Meter		E+H flow meter, with a 0.2 class accuracy.
Electric Control Valve		Zhejiang Ruipu Thermal Electric Actuator, model 381LSB-50, operates in a temperature range from −10 °C to 60 °C, with a stroke of 40 mm.
Pressure Transmitter		E+H Pressure Transmitter, accuracy class 0.5, measuring range 0.2 to 4 MPa.
Data Acquisition System		Wenling Pump Product Testing System, TSJD-001.

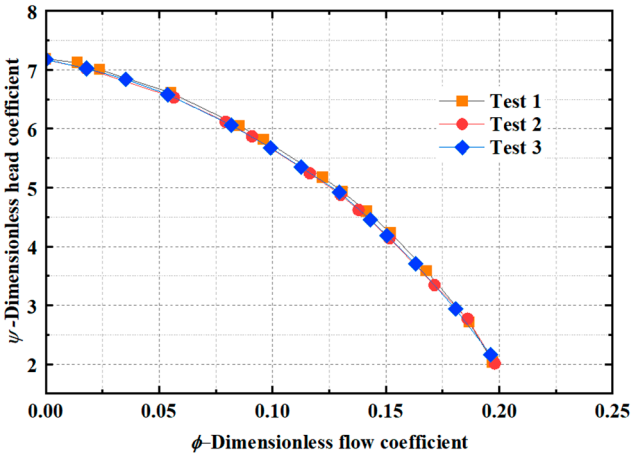
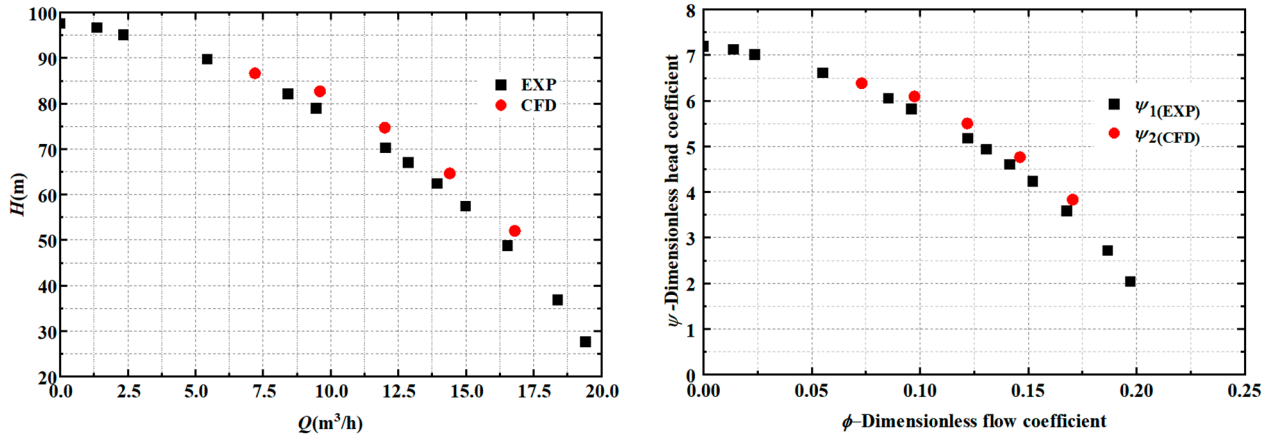


Figure 4. Hydraulic external characteristic repeated trial.

The comparison of flow–head curves from hydraulic tests and numerical simulations for the multistage pump are shown in Figure 5. The maximum error occurs at ϕ = 0.17, amounting to 6.8%. The trend of the simulation curve is consistent with that of the experimental curve, which verifies the correctness of the numerical simulation calculations.



(**a**) (**b**)

Figure 5. Comparison of heads between test and numerical simulation results of the multistage pump. (**a**) Q-H diagram; (**b**) Dimensionless Q-H diagram.

3. Mathematical Models and Numerical Computation Methods

3.1. Control Equation

Given that the fluid was incompressible, the governing equations consisted of the continuity equation and the momentum equation. The Reynolds-averaged Navier-Stokes (RANS) equations can be formulated as:

$$\frac{\partial u_i}{\partial x_i} = 0 \tag{4}$$

$$\frac{\partial}{\partial t}(\rho u_i) + \frac{\partial}{\partial x_j}(\rho u_i u_j) = -\frac{\partial p}{\partial x_i} + \frac{\partial}{\partial x_j}\left[\mu\frac{\partial u_i}{\partial x_j} - \rho\overline{u_i' u_j'}\right] + f_i \tag{5}$$

where u_i and u_j represent the time-averaged velocities in the i and j directions, respectively; x_i and x_j are the displacements in the i and j directions, respectively; p is the time-averaged pressure of the water; ρ is the water density; μ is the dynamic viscosity of the water; and f_i is the body force in the i direction. At 20 °C, ρ = 998 kg/m^3, $\mu = 1.01 \times 10^{-3}$ Pa·s.

3.2. Entropy Production Theory and Computational Equations

To systematically analyze the distribution of flow losses within the multistage pump, entropy production theory was introduced. Entropy production theory is a form of the second law of thermodynamics used to describe the irreversible process of energy dissipation. The entropy production process refers to the inevitable energy conversion effects during this process, where the entropy increment in this irreversible process is always greater than zero, such as the loss of mechanical energy being converted into internal energy. In real flow field systems, entropy production effects also exist. For the flow within a multistage pump, since the specific heat capacity of water is very high, the temperature of the water during the process can be considered constant, so entropy production due to heat transfer is not considered. However, due to the viscosity and turbulence of the flowing water, entropy production and dissipation effects caused by these two irreversible factors exist throughout the flow process. To better reveal the internal energy loss distribution patterns of the multistage pump, this paper analyzed and evaluated it using entropy production theory. For turbulent flow, the Reynolds-averaged entropy production can be divided into

two parts: the viscous dissipation entropy production caused by fluid viscosity and the turbulent dissipation entropy production caused by turbulent fluctuations, which can be calculated by the following formulas [32]:

The total entropy production rate per unit volume is $\dot{S}'''_{\mathrm{D}} = \dot{S}'''_{\overline{\mathrm{D}}} + \dot{S}'''_{\mathrm{D}'}$.

$$\dot{S}'''_{\overline{\mathrm{D}}} = \frac{2\mu}{T}\left[\left(\frac{\partial \overline{u}}{\partial x}\right)^2 + \left(\frac{\partial \overline{v}}{\partial y}\right)^2 + \left(\frac{\partial \overline{w}}{\partial z}\right)^2\right] + \frac{\mu}{T}\left[\left(\frac{\partial \overline{u}}{\partial y} + \frac{\partial \overline{v}}{\partial x}\right)^2 + \left(\frac{\partial \overline{u}}{\partial z} + \frac{\partial \overline{w}}{\partial x}\right)^2 + \left(\frac{\partial \overline{v}}{\partial z} + \frac{\partial \overline{w}}{\partial y}\right)^2\right] \tag{6}$$

$$\begin{aligned}\dot{S}'''_{\mathrm{D}'} = {} & \frac{2\mu_{\mathrm{eff}}}{T}\left[\left(\frac{\partial u'}{\partial x}\right)^2 + \left(\frac{\partial v'}{\partial y}\right)^2 + \left(\frac{\partial w'}{\partial z}\right)^2\right] \\ & + \frac{\mu_{\mathrm{eff}}}{T}\left[\left(\frac{\partial u'}{\partial y} + \frac{\partial v'}{\partial x}\right)^2 + \left(\frac{\partial u'}{\partial z} + \frac{\partial w'}{\partial x}\right)^2 + \left(\frac{\partial v'}{\partial z} + \frac{\partial w'}{\partial y}\right)^2\right]\end{aligned} \tag{7}$$

where $\overline{u}$, $\overline{v}$, $\overline{w}$ are the components of the mean velocity in the x, y, and z directions, respectively, m/s; u', v', and w' are the components of the fluctuating velocity in the x, y, and z directions, respectively, m/s; T is the temperature, K; and μ is the dynamic viscosity of the fluid, Pa·s. The mean velocity components $\dot{S}'''_{\overline{\mathrm{D}}}$ can be directly obtained through numerical calculation, whereas the fluctuating velocity components $\dot{S}'''_{\mathrm{D}'}$ cannot be solved due to the difficulty in obtaining the turbulent velocity field. Kock et al. [33] suggested that there is an intrinsic connection between turbulent dissipation entropy production and the turbulence model, and it is related to the turbulent kinetic energy dissipation rate ω and turbulence intensity k. Therefore, in the k-ω turbulence model, the turbulent entropy production rate caused by turbulent fluctuations can be rewritten as:

$$\dot{S}'''_{\mathrm{D}'} = \beta\frac{\rho\omega k}{T} \tag{8}$$

where the empirical coefficient β is determined through direct numerical simulation calibration and was taken as 0.09.

By integrating the viscous dissipation entropy production rate and the turbulent dissipation entropy production rate over the volume, the following results are obtained:

$$S_{\mathrm{DV}} = \int_V \dot{S}'''_{\overline{\mathrm{D}}} dV \tag{9}$$

$$S_{\mathrm{DT}} = \int_V \dot{S}'''_{\mathrm{D}'} dV \tag{10}$$

where S_{DV} is the viscous dissipation entropy production, W/K; S_{DT} is the turbulent dissipation entropy production, W/K; and V is the volume of the computational domain. The entropy production rate exhibits a strong wall effect. According to the wall friction loss calculation method proposed by Zhang et al. [34], the wall dissipation entropy production S_{W} can be obtained by integrating as follows:

$$S_{\mathrm{W}} = \int_S \frac{\tau v}{T} dS \tag{11}$$

where τ is the wall shear stress, Pa; S is the area, m^2; and v is the near-wall velocity, m/s.

The total entropy production of the entire fluid computational domain is:

$$S = S_{\mathrm{DV}} + S_{\mathrm{DT}} + S_{\mathrm{W}} \tag{12}$$

4. Computational Results and Analysis

4.1. Comparison of Different Types of Entropy Production

Local entropy production is primarily categorized into three types: viscous dissipation entropy production S_{DV}, turbulent dissipation entropy production S_{DT}, and wall dissipation entropy production S_W. To better analyze the types of entropy production in a multistage pump under different flow conditions, Figures 6 and 7 respectively illustrate the values and percentage distributions of various types of entropy production.

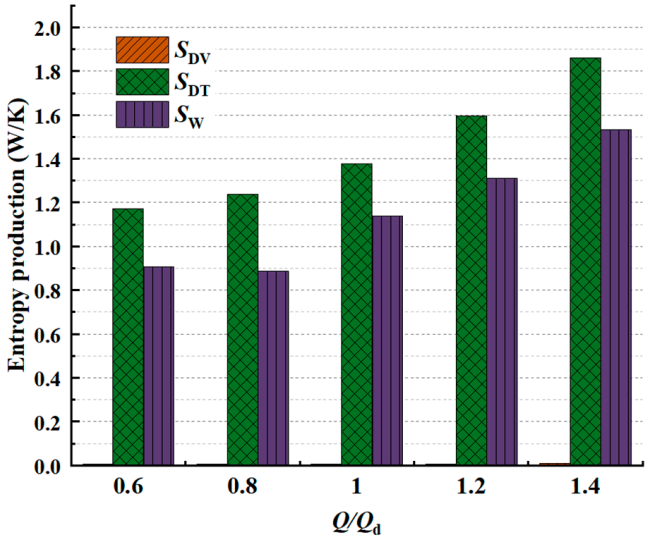


Figure 6. Entropy production of different types.

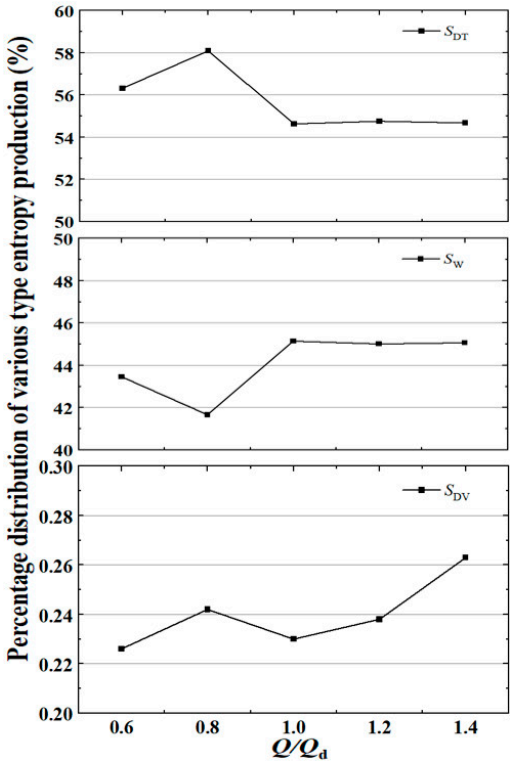


Figure 7. Percentage distributions of various types of entropy production under different flow rates.

In Figure 6, it can be observed that both turbulent dissipation entropy production and wall dissipation entropy production increase as the flow rate increases, indicating a

rise in internal energy losses within the multistage pump corresponding to higher flow rates. By observing the entropy production percentage distribution, the viscous dissipation entropy production is consistently below 0.28% under all flow conditions. At $1.4Q_d$, this percentage reaches a maximum value of 0.263%. Conversely, the proportions of turbulent dissipation entropy generation and wall dissipation entropy generation are significantly greater under various flow conditions. Specifically, the percentage of turbulent dissipation entropy production is greater than 54% under all flow conditions, reaching its maximum value of 58.096% at $0.8Q_d$. The percentage of wall dissipation entropy production is smallest at $0.8Q_d$ but still reaches 41.66%.

Thus, turbulent dissipation entropy generation and wall dissipation entropy generation were deemed the primary causes of energy loss in the operation of the multistage pump, with viscous dissipation entropy generation being negligible. A similar phenomenon is also mentioned in the literature of Hou et al. [15].

4.2. Comparison of Entropy Production in Various Flow Components

Figure 8 shows the percentage distributions of entropy production for impellers, diffusers, the inlet chamber, and the outlet chamber under different flow rates. From the percentage distribution of entropy production of each flow component, it is discernible that, with the increase in flow rate, the entropy production associated with the impeller exhibits an initial decline, followed by an augmentation. At low flow rates, the entropy production of the impeller changes very little, within 1%, while at high flow rates, the entropy production changes by more than 3%. The trend for diffusers is the opposite, showing an initial increase followed by a decrease. The percentage distribution of entropy production of the inlet chamber remains around 1%, maintaining a relatively low level. Overall, the diffusers are the primary area of energy dissipation within the multistage pump, followed by the impellers and outlet chamber. At the design flow rate, the impeller loss accounts for 13.5%, the outlet chamber loss for 10.1%, and the diffuser loss for 74.4%. A similar phenomenon is also mentioned in the literature of Fan et al. [35]. Therefore, these three components are the key areas for hydraulic loss in multistage pumps.

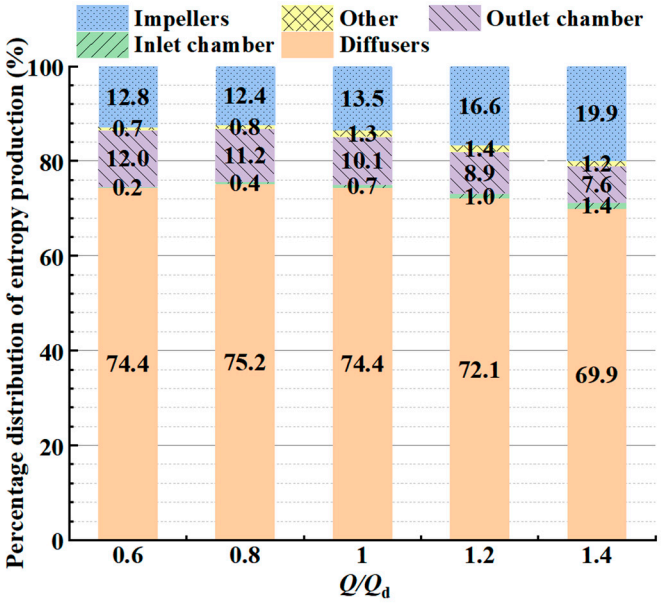
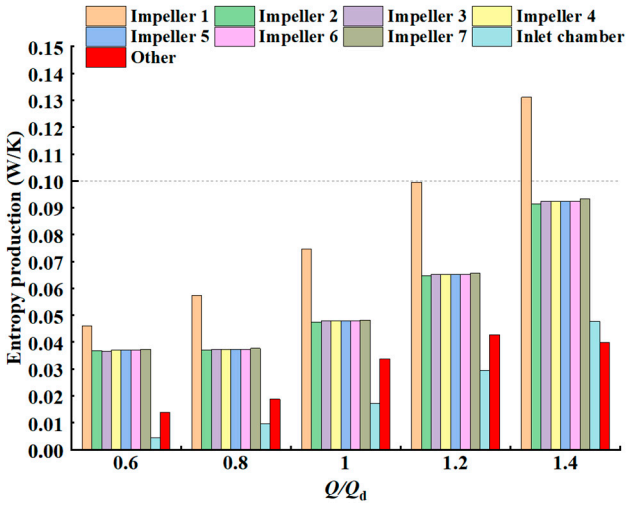


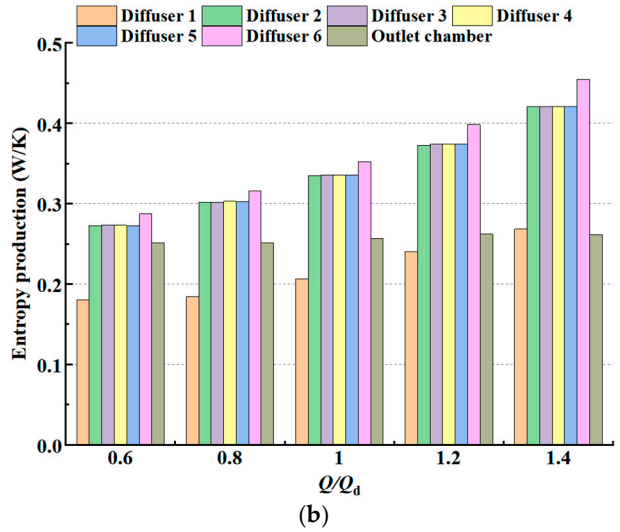
Figure 8. Entropy production of different flow components under different flow rates.

To delve deeper into the energy losses across each flow element of the multistage pump at varying flow rates, calculations were performed for the entropy production of each impeller and diffuser stage. In Figure 9a, it can be observed that the energy loss trends in the inlet chamber and impellers are almost identical, and the entropy production

value increases with the increase in flow rate. The significant difference is that the entropy production of the inlet chamber is much lower, while the entropy production of the impeller is significantly higher. Notably, among the impeller domains, the entropy production values of impeller 2 to impeller 7 are close under different flow rates, while the entropy production value of impeller 1 is significantly higher than that of the other impellers. At $1.4Q_d$, the entropy production value of impeller 1 is 25% higher than that of the other impellers. In Figure 9b, it can be clearly seen that the entropy production in the outlet chamber remains almost unchanged with varying flow rates, maintaining a value of around 0.25 W/K. Overall, the entropy production in the outlet chamber is relatively high, which may be due to the turbulent flow state after the fluid passes through multiple flow components. Within the diffuser regions, the entropy production remains relatively consistent for diffuser 2 through diffuser 5 across various flow rates. In contrast, diffuser 1 and diffuser 6 exhibit significantly different entropy production levels. Diffuser 1 consistently shows entropy production approximately 60% less than the others, whereas diffuser 6 typically records higher values.



(**a**)



(**b**)

Figure 9. Entropy production of each flow component under different flow rates. (**a**) Impellers and other flow components; (**b**) Diffusers and the outlet chamber.

4.3. Entropy Production Distribution at Different Cross Sections

Based on the above studies, it can be observed that the entropy production value of impeller 1 is significantly higher than that of the other impellers. In order to analyze this phenomenon further, the internal flow states of impeller 1 and impeller 2 were studied under the design flow rate. As shown in Figure 10, three sections of the impeller were selected, corresponding to 0.05 times (Section A), 0.5 times (Section B), and 0.95 times (Section C) of the impeller outlet width. Figure 11 displays the local entropy production rate across various sections of the impellers. It is clear from the figure that the local entropy production rate in impeller 1's flow path is unevenly distributed. In all sections, the local entropy production rate of impeller 1 is higher than that of impeller 2, and the features in section A and section C are particularly obvious.

It is also noteworthy that the local entropy production values at the inlet and outlet of the channels of impeller 1 are significantly higher than those in other areas. Since the geometric parameters of the impellers are the same, this difference is attributed to the different inflow conditions. There is an annular inlet chamber connected to the upstream of impeller 1, which cannot provide uniform axisymmetric inflow conditions, resulting in turbulence in the inlet flow of impeller 1. This results in a certain circumferential velocity and causes the impeller to be subjected to fluid impact at the inlet, leading to greater impact losses and consequently higher energy loss. In contrast, a diffuser is connected upstream of impeller 2, and the diffuser plays a rectifying role, reducing the impact of inlet flow turbulence and resulting in lower energy losses.



Figure 10. Impeller cross section diagram.

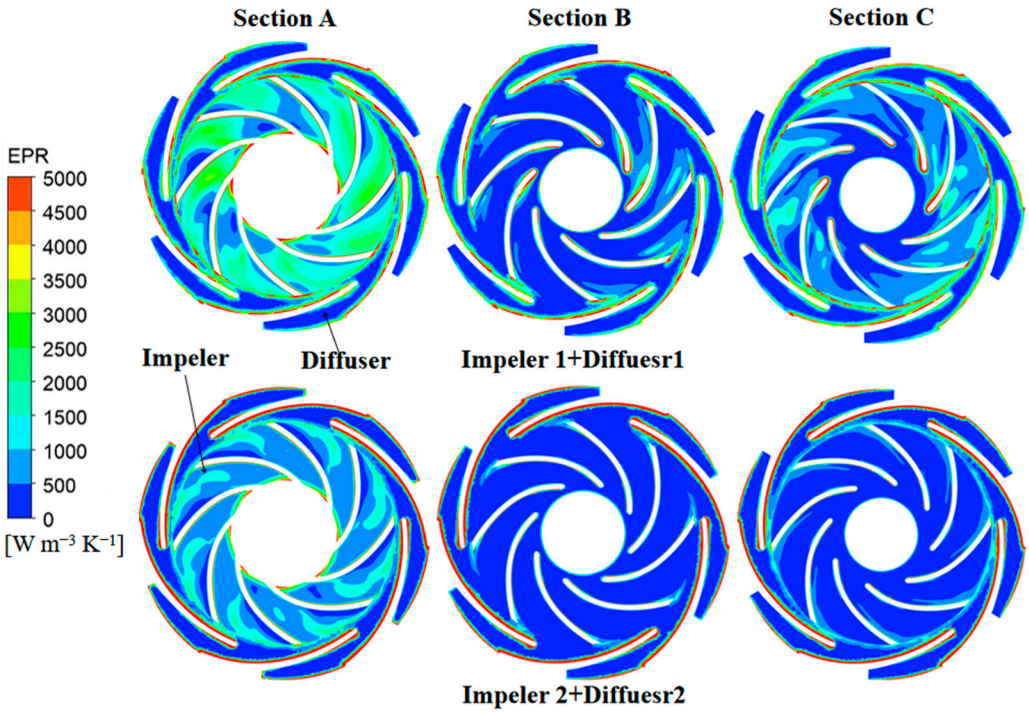


Figure 11. Distribution of entropy production rates under different impellers and diffusers.

In a multistage pump, the diffuser is composed of a forward diffuser, transition section, and backward diffuser. It can be seen from Figure 11 that in the front diffuser flow channels, the local entropy production rates of diffuser 1 and diffuser 2 do not change much. In order to further analyze the energy loss in the entire diffuser, diffuser 1 and diffuser 2 were selected as the research objects because the entropy production distributions of diffuser 2 to other diffusers are not much different, as shown in Figure 9b.

Figure 12 depicts the streamline patterns within the reverse flow channels of diffuser 1 and diffuser 2. The streamlines within diffuser 1 closely adhere to the contour, with instability and local flow detachment occurring only at the channel exit and the subsequent impeller entry. In contrast, diffuser 2 exhibits a substantial velocity gradient, creating a low-speed region in the channel's midsection. Moreover, complex flow dynamics occur at the diffuser outlet and the next impeller inlet. An enlarged view reveals that, due to the significant velocity gradient, a pair of counter-rotating vortices emerge in this area. In summary, the appearance of the vortex increases the degree of chaos inside diffuser 2, intensifies the turbulent pulsation, and causes a significant increase in its entropy production value.

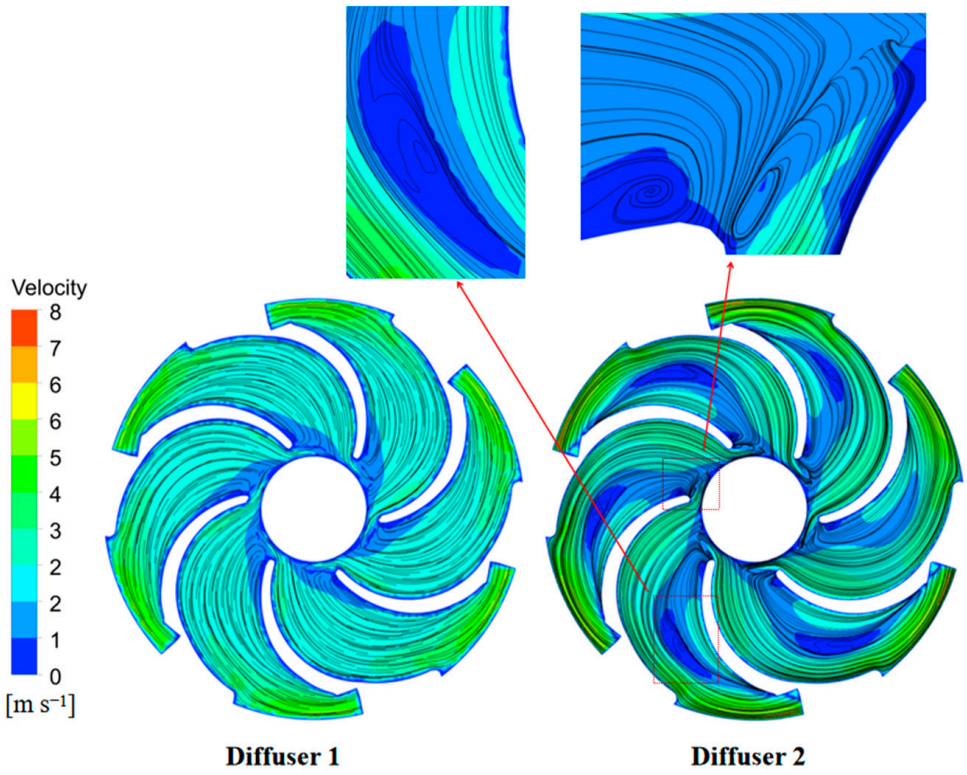


Figure 12. Velocity line of the middle section of the return diffuser.

The impeller is the core flow component of the multistage pump. In order to analyze in detail the entropy production distribution in different stream surfaces of the impeller under different flow rates, three span surfaces of impeller 1 were selected. The span 0.05 is located near the hub of the impeller, span 0.5 corresponds to the middle stream surface of the impeller, and span 0.95 is located near the shroud of the impeller, as shown in Figure 13.



Figure 13. Stream surface of spans 0.05, 0.5, and 0.95 in the span-wise direction.

Figure 14 illustrates the distribution of entropy production rates across various spans of impeller 1 at different flow rates. Regions of high entropy production are predominantly found at the impeller inlet, the blade leading edge, the suction side of the blade, and the impeller outlet. With an increase in flow rate, these high entropy production zones expand, aligning with the overall pattern observed in Figure 9 regarding the impeller entropy production under varying flow conditions. Additionally, it can be observed that the entropy production distribution exhibits some similarities across different span sections. Under low flow rates, the distribution region of the high entropy production rate is concentrated in the blade inlet region, and as the flow rate increases, this region expands downstream, resulting in an increase in entropy production in the impeller outlet region. The main reason is that a significant flow impact occurs in the blade inlet region (as shown in the local magnification in Figure 15), causing severe impact losses and resulting in a high entropy production rate in the impeller inlet region. As the flow rate increases, the entropy production rate at the impeller outlet significantly increases, indicating that the increase in the flow rate causes a noticeable jet wake to form in the impeller outlet region (as shown in Figure 16), resulting in wake losses and more chaotic flow. A similar phenomenon is also mentioned in the literature of Wu et al. [36]. It is worth noting that at span 0.95, that is, close to the shroud area of the impeller, a large region with high entropy production rate also appears in the impeller inlet region. Moreover, as the span approaches the hub region, the entropy production rate value in the impeller inlet region significantly decreases. The reason may be that the velocity distribution in the hub area is more uniform than that at the impeller inlet, reducing turbulence and the entropy production rate due to the velocity gradient. In addition, the blades may have a stronger guiding effect on the fluid in the hub area, which helps to reduce flow losses and thus reduce the entropy production rate.

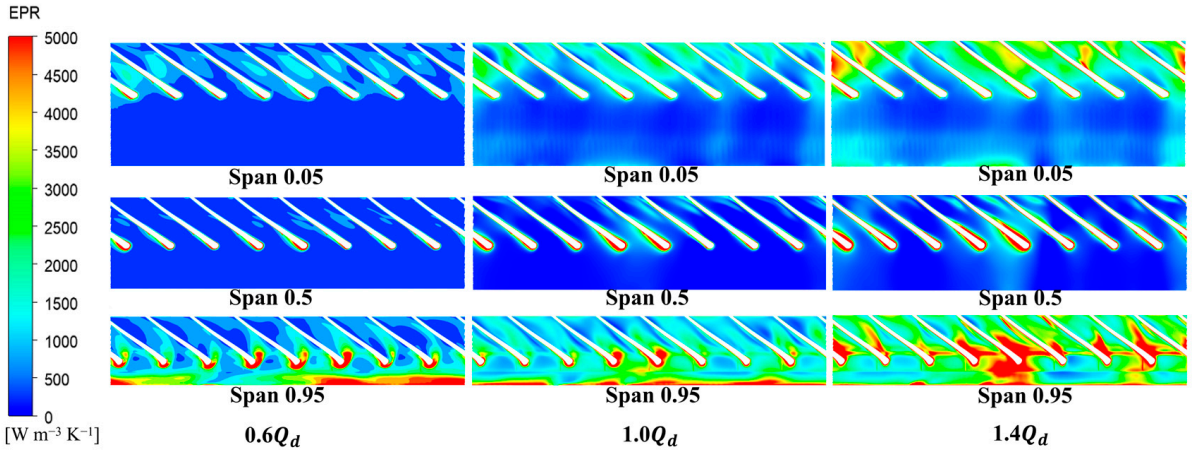


Figure 14. Entropy production rate distribution at different spans of impeller 1 under different flow rates.

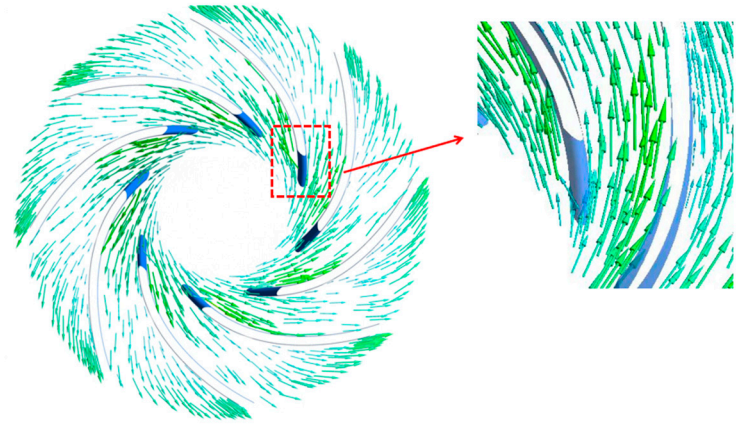


Figure 15. Relative velocity vector.

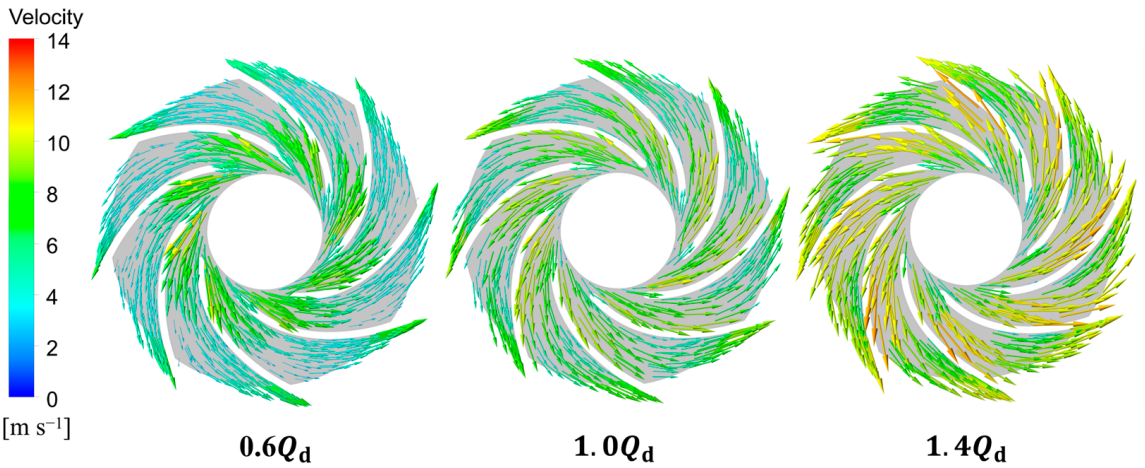


Figure 16. Relative velocity vector under different flow rates.

To provide additional insight into the cause of elevated entropy production in the impeller, Figure 17 displays the vortex structures within impeller 1 at various flow rates. As indicated in Figure 9, impeller 1 exhibits notably higher entropy production compared to the other impellers. The vortex identification is conducted using the Q-Criterion vortex core detection method, so this study analyzed the vortex core distribution at Q = 0.04 and used turbulent kinetic energy to color the surface.

From the distribution of vortex cores inside the multistage pump, the vortex cores are mainly concentrated in the impeller inlet and impeller outlet regions. At the impeller inlet, there are a ring-shaped vortex core and an axial vortex core. The ring-shaped vortex core is distributed along the inner wall of the shroud of the impeller, while the axial vortex core is located along the wall of the hub of the impeller. The inertial force of the fluid may have a greater impact at the impeller inlet, especially in high-speed rotating impellers, where the circular motion of the fluid may cause the axial and annular flows to separate and form the vortex core. As the flow rate increases, the number of vortex cores with high turbulent kinetic energy gradually increases, especially at the impeller outlet. This phenomenon may be due to the intensified jet-wake phenomenon at the impeller outlet as the flow rate increases.

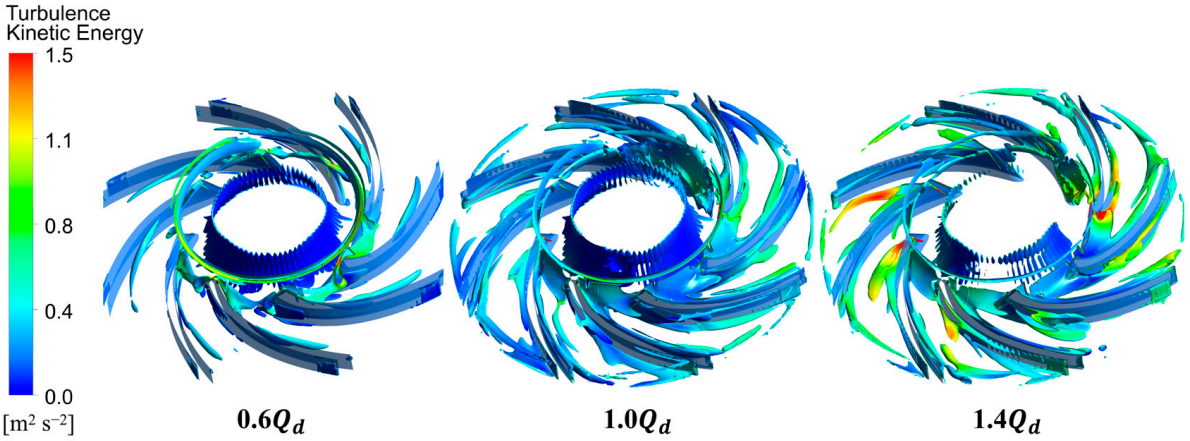


Figure 17. Vortex distribution inside the impeller under different flow rates.

As shown in Figure 9, the diffusers are also the critical area of hydraulic losses in the multistage pump. The entropy production distributions of diffuser 1, diffuser 2, and diffuser 6 show certain differences. In order to further quantify the spatial difference in the entropy production rate, the diffuser was divided into 11 cross sections along the axial direction, as shown in Figure 18a. In the axial section, the transition section is located in the middle position, that is, the sixth section in Figure 18b (X = 0.00 m). Section 3 to section 5 are sections passing through the impeller outlet area, and section 7 to section 9 are sections passing through the main diffuser. The distance between adjacent sections is 0.004 m.

Figure 18b shows the distribution of the area-averaged entropy production rate in different axial cross sections of three different diffusers at the design flow rate. With the exception of the initial cross section of diffuser 1, which exhibits a higher area-averaged entropy production rate than diffuser 2 and diffuser 6, the remaining cross sections have lower area-averaged entropy production rates than diffuser 2 and diffuser 6, indicating that the energy loss of diffuser 1 is significantly less than that of diffuser 2 and diffuser 6. The changes in the area-averaged entropy production rates of diffuser 2 and diffuser 6 in different axial sections are roughly similar. Only in a few cross sections, the area-averaged entropy production rates of diffuser 6 are slightly higher than those of diffuser 2, which is consistent with the entropy production patterns of the different diffusers shown in Figure 9. It is worth noting that the area-averaged entropy production rates in the sections close to the impeller outlet area (i.e., Section 3 to Section 5) are much higher than those in other sections. This is due to the dynamic and static interference caused by the interaction between the impeller outlet area and the diffuser.

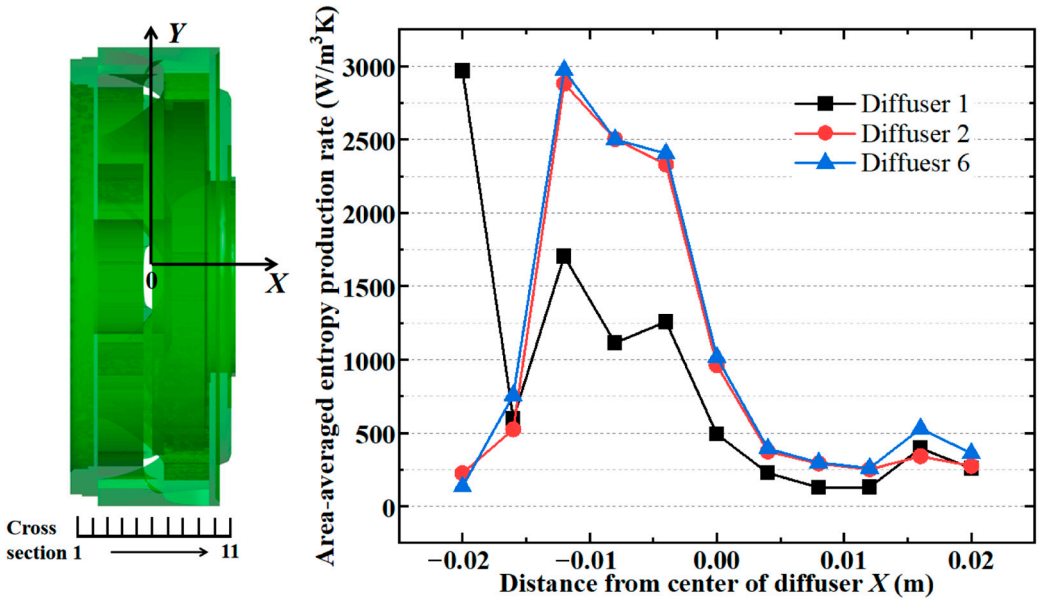


Figure 18. Entropy production rate distribution at different cross sections in the first diffuser. (**a**) Positions of different cross sections. (**b**) Area-averaged entropy production rates in different axial cross sections of three different diffusers.

5. Conclusions

Based on entropy production theory and the Q-Criterion, the influence of different flow components, impellers, and diffusers at different stages on the internal flow characteristics of the pump is revealed, providing a basis for the optimal design of multistage pumps. The main conclusions of the paper are as follows:

(1) The entropy production losses inside the multistage pump are mainly caused by turbulent dissipation entropy production and wall dissipation entropy production, while the viscous dissipation entropy production is relatively small. The impellers and diffusers are the main regions of energy loss, accounting for a high proportion of the total loss. At the design flow rate, the energy loss in the diffusers is the largest, accounting for 75.2%.

(2) Energy loss in the impellers is primarily concentrated at the blade inlet region, blade suction surface, impeller outlet region, and impeller inlet region. With rising flow rates, the areas of intense entropy production enlarge. At lower flow rates, these areas are focused at the blade inlet. However, as the flow rate increases, these regions of high entropy production extend further downstream. This is mainly due to a significant flow impact at the blade inlet region, causing severe impact losses and a higher entropy production rate at the impeller inlet region. As the flow rate increases, there is an obvious jet wake at the impeller outlet, leading to wake loss and a significant increase in the entropy production rate. Meanwhile, as the span nears the hub region, the entropy production rate in the impeller inlet drops due to a more uniform velocity distribution reducing turbulence and velocity gradient-related entropy production.

(3) Except for diffuser 1, low-speed areas appeared in the flow channels of the backward diffusers of the other diffusers, resulting in the formation of vortices. Complex flow phenomena also appeared from the diffuser outlet area to the downstream impeller inlet area. The appearance of vortices increased the degree of turbulence and chaotic flow in the diffusers, which significantly increased the entropy production value.

Author Contributions: Q.M.: conceptualization, methodology, and writing—original draft. G.L.: writing—review, supervision, and editing. J.M.: supervision and editing. D.Z.: validation. Y.L.: validation. T.H.: data curation. All authors have read and agreed to the published version of the manuscript.

Funding: This work was supported by the Natural Science Foundation of Jiangsu Province (Grant No. BK20210761), Special Supported Project of China Postdoctoral Science Foundation (Grant No. 2021TQ0130), the Self-supported Project of Wenling Fluid Machinery Technology Institute of Jiangsu University (Grant No. 01012). and Taizhou City Social Development Science and Technology Plan Project (Grant No. 23sfb07).

Data Availability Statement: The data that have been used are confidential.

Conflicts of Interest: The authors declare that the research was conducted in the absence of any commercial or financial relationships that could be construed as a potential conflict of interest.

Glossary

Nomenclature

H_d	Design head (m)
n	Rotational speed (rpm)
S_{DV}	Direct dissipation entropy production (W/K)
S_{DT}	Turbulent dissipation entropy production (W/K)
S_{W}	Wall entropy production (W/K)
S	Total entropy production (W/K)
Q_{d}	Design flow rate (m^3/h)
η	Efficiency (%)
ϕ	Dimensionless flow coefficient
Ψ	Dimensionless head coefficient
u_2	Impeller outlet circumference speed (m/s)
ρ	Fluid density (kg/m^3)
μ	Dynamic viscosity of the fluid (Pa·s)
$\dot{S}'''_{\overline{D}}$	Entropy production rate induced by average velocity ($W \cdot m^{-3}/K$)
$\dot{S}'''_{D'}$	Entropy production rate induced by fluctuating velocity ($W \cdot m^{-3}/K$)
μ_{eff}	Effective dynamic viscosity (Pa·s)

Abbreviations

CFD	Computational fluid dynamics
CMEI	Auxiliary variables of minimum efficiency index
LES	Large eddy simulation
RN	Re-normalization group
RBF	Radial basis function
MRF	Multiple reference frame
RANS	Reynolds-averaged Navier-Stokes

References

1. Jafarzadeh, B.; Hajari, A.; Alishahi, M.M.; Akbari, M.H. The flow simulation of a low-specific-speed high-speed centrifugal pump. *Appl. Math. Model* **2010**, *35*, 242–249. [CrossRef]
2. Ji, P.; Shouqi, Y.; Jianping, Y. Numerical analysis of periodic flow unsteadiness in a single-blade centrifugal pump. *Sci. China Technol. Sci.* **2012**, *56*, 212–221.
3. Weidong, S.; Ling, Z.; Weigang, L.; Bing, P.; Tao, L. Numerical prediction and performance experiment in a deep-well centrifugal pump with different impeller outlet width. *Chin. J. Mech. Eng.* **2013**, *26*, 46–52.
4. Mingao, T.; Huan, X.; Houlin, L.; Xianfang, W.; Jianbao, C. Analysis of head prediction of centrifugal pumps at low flow rate based on CFD. *Chin. J. Mech. Eng.* **2013**, *29*, 31–36.
5. Eun, L.S.; Hyun, S.C. CFD analysis of performance change in accordance with inner surface roughness of a double-entry centrifugal pump. *J. Mech. Sci. Technol.* **2018**, *32*, 697–702.
6. Lulu, Z.; Xiaoping, C.; Huashu, D.; Wei, Z.; Zuchao, Z.; Xueli, C. Effects of clearance flow on the characteristics of centrifugal pump under low flow rate. *J. Mech. Sci. Technol.* **2020**, *34*, 189–200.
7. Baoling, C.; Yingbin, Z.; Yakun, H.; Zuchao, Z. Analysis of unsteady flow and fluid exciting forces of multistage centrifugal pump based on actual size. *Proc. Inst. Mech. Eng. Part A* **2022**, *236*, 21–32.

8. Tianxin, W.; Denghao, W.; Shuyu, G.; Yu, S.; Yun, R.; Jiegang, M. Multi-objective optimization and loss analysis of multistage centrifugal pumps. *Energy* **2023**, *284*, 128638.
9. Lei, Z.; Dayong, W.; Yang, G.; Qiang, P.; Weidong, S.; Rujie, Z. Optimization of hydraulic efficiency and internal flow characteristics of a multi-stage pump using RBF neural network. *Water* **2024**, *16*, 1488. [CrossRef]
10. Hongtao, Z.; Chenbiao, T.; Yun, L. Study on the influence of different inflow on the internal flow stability of centrifugal pump. *Chin. J. Mech. Eng.* **2024**, *42*, 881–887.
11. Chao, C.; Hu, X.; Fanjie, D.; Kaipeng, W.; Zhang, Z.; Qiaorui, S. Study on the transient flow characteristics of multistage centrifugal pumps during the startup process before system operation. *Water* **2024**, *16*, 1876. [CrossRef]
12. Shu, X.; Ren, Y.; Denghao, W.; Zhibing, Z.; Jiegang, M. Energy loss and unsteady flow characteristics in a self-priming pump. *J. Hydraul. Eng.* **2019**, *50*, 1010–1020.
13. Deyou, L.; Ruzhi, G.; Hongjie, W.; Gaoming, X.; Xianzhu, W.; Daqing, Q. Entropy production analysis for hump characteristics of a pump turbine model. *Chin. J. Mech. Eng.* **2016**, *29*, 803–812.
14. Xiaojun, L.; Zuchao, Z.; Yi, L.; Xiaoping, C. Experimental and numerical investigations of head-flow curve instability of a single-stage centrifugal pump with volute casing. *Proc. Inst. Mech. Eng. Part A* **2016**, *230*, 633–647.
15. Hucan, H.; Yongxue, Z.; Zhenlin, L.; Ting, J.; Jinya, Z.; Cong, X. Numerical analysis of entropy production on a LNG cryogenic submerged pump. *Gas. Sci. Eng.* **2016**, *36*, 87–96.
16. Deyou, L.; Hongjie, W.; Yonglin, Q.; Lei, H.; Xianzhu, W.; Daqing, Q. Entropy production analysis of hysteresis characteristic of a pump-turbine model. *Energ. Convers. Manag.* **2017**, *149*, 175–191.
17. Hongyu, G.; Wei, J.; Jianguo, Y.; Yuchuan, W.; Xinghai, Z.; Junxue, W. Energy loss analysis of the double-suction centrifugal pump under different flow rates based on entropy production theory. *Proc. Inst. Mech. Eng. Part C* **2020**, *234*, 4009–4023.
18. Ran, T.; Zengwei, W. Comparative numerical studies for the flow energy dissipation features in a pump-turbine in pump mode and turbine mode. *J. Energy. Storage* **2021**, *41*, 102835.
19. Zhifeng, Y.; Wenquan, W.; Yan, Y.; Xingshun, L. Energy loss evaluation in a Francis turbine under overall operating conditions using entropy production method. *Renew. Energy* **2021**, *169*, 982–999.
20. Yefu, W.; Yang, W.; Jianlong, S.; Shibin, J.; Xuran, G.; Rui, Z.; Puyu, C. Numerical study on influence of elbow installation angle on pressure fluctuation in pipeline pump. *Chin. J. Mech. Eng.* **2022**, *40*, 1219–1226.
21. Xiaolin, W.; Yong, W.; Houlin, L.; Yadong, X.; Linglin, J.; Ming, L. A numerical investigation on energy characteristics of centrifugal pump for cavitation flow using entropy production theory. *Int. J. Heat. Mass. Transf.* **2022**, *201*, 123591.
22. Yongxue, Z.; Hucan, H.; Chang, X.; Wenxuan, H.; Zhenlin, L. Application of entropy production method to centrifugal pump energy loss evaluation. *J. Drain. Irrig. Mach. Eng.* **2017**, *35*, 277–282.
23. Fan, Z.; Shouqi, Y.; Xueyuan, W.; Ke, C. Study on flow loss characteristics of side channel pump based on entropy production. *Chin. J. Mech. Eng.* **2018**, *54*, 137–144.
24. Xiaoqi, Z.; Zuchao, Z.; Xiaoli, Y.; Yuliang, Z. Internal unsteady flow characteristics of centrifugal pump based on entropy generation rate and vibration energy. *Proc. Inst. Mech. Eng. Part E* **2018**, *233*, 456–473.
25. Cao, J.; Pei, J.; Gu, Y.; Wang, W.; Yuan, S. Flow losses analysis in a mixed flow pump with annular volute by entropy production evaluation. *IOP Conf. Ser. Earth Environ. Sci.* **2019**, *240*, 032047. [CrossRef]
26. Jianyuan, L.; Wenqian, X.; Yuan, Z.; Longhai, L.; Huashu, D. The influence of volute tongue angle on the characteristic and flow stability of the centrifugal pump. *J. Zhejiang. Univ. Sci. A.* **2021**, *45*, 351–364.
27. Bing, Q.; Desheng, Z.; Linlin, G.; Ruijie, Z.; van Esch, B.P.M. Numerical and experimental investigations on inflow loss in the energy recovery turbines with back-curved and front-curved impeller based on the entropy generation theory. *Energy* **2021**, *239*, 122426.
28. Shaoguang, Z.; Jianwei, H.; Yuhui, S.; Yang, Y.; Danyang, D.; Xiangyu, S.; Ling, Z. Internal flow characteristics of electrical submersible pump based on numerical simulation and entropy production theory. *Chin. J. Mech. Eng.* **2023**, *41*, 771–778.
29. Goto, A.; Zangeneh, M. Hydrodynamic design of pump diffuser using inverse design method and CFD. *J. Fluids. Eng.* **2002**, *124*, 319–328. [CrossRef]
30. Leqin, W.; Dazhuan, W.; Shuiying, Z.; Yuzheng, H. Study on transient hydrodynamic performance of mixer-flow-pump during starting period. *J. Zhejiang. Univ. (Eng. Sci.)* **2004**, *38*, 751–755.
31. Congxin, Y.; Bin, W. 3-D Numerical simulation on transient characteristics of a multistage centrifugal pump during starting period. In *Power and Energy Engineering Conference (PEEC 2010 E-BOOK)*; Lanzhou University of Technology: Lanzhou, China, 2010; pp. 177–181.
32. Bejan, A. *The Method of Thermodynamic Optimization of Finite-Size Systems and Finite-Time Processes. Entropy Generation Minimization*; CRC Press: Boca Raton, FL, USA, 1995; Volume 117–118.
33. Kock, F.; Herwig, H. Local entropy production in turbulent shear flows: A high-Reynolds number model with wall functions. *Int. J. Heat Mass Transf.* **2004**, *47*, 2205–2215. [CrossRef]
34. Xiang, Z.; Yang, W.; Xiaomin, X.; Hongyu, W. Energy conversion characteristic within impeller ofLow specific speed centrifugal pump. *Trans. CSAE* **2011**, *42*, 75–81.

35. Baoxin, F.; Zhaoyu, L.; Ruonan, F.; Songying, C. Numerical study on entropy generation of the multi-stage centrifugal pump. *Entropy* **2022**, *24*, 923. [CrossRef] [PubMed]
36. Xiaohui, W.; Huzhong, J.; Senchun, M.; Xiaobang, B.; Bing, Q. Analysis of energy dissipation mechanism of multistage hydraulic turbine based on entropy production theory. *Trans. CSAE* **2024**, *55*, 162–172.

Disclaimer/Publisher's Note: The statements, opinions and data contained in all publications are solely those of the individual author(s) and contributor(s) and not of MDPI and/or the editor(s). MDPI and/or the editor(s) disclaim responsibility for any injury to people or property resulting from any ideas, methods, instructions or products referred to in the content.